New bioresorbable filaments for scaffolds intending local sodium alendronate release

Olivia Deretti[1]* [iD], Guilherme Tait[2] [iD], Lucas Werner[3] [iD], Luana Engelmann[2] [iD],
Denise Abatti Kasper Silva[1] [iD] and Ana Paula Testa Pezzin[1] [iD]

[1] *Laboratório de Materiais, Programa de Mestrado em Engenharia de Processos,Universidade da Região de Joinville – UNIVILLE, Joinville, SC, Brasil*
[2] *Laboratório de Materiais, Departamento de Engenharia Química, Universidade da Região de Joinville – UNIVILLE, Joinville, SC, Brasil*
[3] *Laboratório de Materiais, Departamento de Engenharia Mecânica, Universidade da Região de Joinville – UNIVILLE, Joinville, SC, Brasil*

*oliviaderetti@hotmail.com

Abstract

Scaffolds with osteoconductivity, biocompatibility and good mechanical properties are promising for local drug release of sodium alendronate (ALN), a first-choice drug for treatment of bone tissue diseases, with low bioavailability. The viability to manufacture poly (L-lactic acid) (PLLA)/poly (methyl methacrylate) (PMMA) filaments containing ALN in different proportions, through extrusion, followed by scaffolds using 3D printing by fusion deposition modelling (FDM) and to investigate the influence of processes in mixtures drove this study. Differential scanning calorimetry (DSC), spectroscopy in the infrared region with Fourier transform (FTIR/ATR), and X-ray diffractometry (XRD) analysis indicated that PMMA decelerates crystallinity and confers malleability to PLLA/ALN mixture, besides its good processability and miscibility with PLLA and no relevant changes in physicochemical properties of components. Field emission scanning electron microscopy (SEM/FEG) showed good interfacial compatibility between PLLA/PMMA and homogeneously dispersed drug crystals in matrix. PLLA-PMMA-ALN scaffolds were manufactured by accurate with interesting properties for bone tissue engineering.

Keywords: *filaments characteristics, polyesters, second generation bisphosphonate.*

1. Introduction

Sodium Alendronate (ALN) is used to various bone tissue disorders such as osteoporosis, Paget disease, bone cancer and bone metastases[1]. This drug has a great affinity for the human bone matrix and can inhibit resorption and increase bone formation[1]. However, the ALN has low bioavailability (<1%) and requires high doses via oral or intravenous administration generating side effects.

The administration of medication at the local level can minimize negative effects[2], reduce the dosages to required therapeutic levels, increase patient compliance, and improve the patient's quality of life[3]. Scaffolds with osteoconductivity and osteoinductivity are promising alternatives to perform this function and solve challenges such as complex bone geometry, surgery needs, and risks of infection. The scaffolds must possess strong mechanical properties, biocompatibility, and degrade gradually while new tissue and extracellular matrix are formed and must have high porosity and interconnected pores[4]. They are a kind of implantable system that acts as a means of efficacy local drug administration resulting in high drug concentrations

at the site of interest, reducing systemic drug exposure[5] been classified as a pharmaceutical dosage forms and medical devices[6].

Three-dimensional printing (3DP) is a modern way to produce scaffolds incorporating drugs and the fusion deposition modeling (FDM) method, a regular process that allows fabricate different structures design with interconnected macropore sizes according to demands[2]. This method dispenses solvents and is low-cost[7]. For the 3D printer, filaments produced from pure, or a mixture of materials feed the printer and enable continuous process but can also degrade the components[8]. A key point is to select appropriate parameters[8,9] such as screw speed, extruder feed, and temperature are crucial, as well as incorporating flow agents to increase the component fluidity index[10,11].

PLLA is one of the most used materials in FDM-3DP due to its easy-to-process properties by extrusion, high mechanical resistance, and low thermal expansion coefficient[12]. It has been approved by the American regulatory agencies (FDA) and European Medicine Agency (EMA) for application in

pharmaceutical and medicinal areas, notably because it is bioresorbable, biocompatible, and has low immunogenicity[13,14].

To improve thermomechanical and flow properties and regulate PLLA crystallization, poly (methyl methacrylate) (PMMA) is an alternative due to the compatibility between them and because its mixture can structure a mechanical entanglement of molecular chains after fusion[15]. The PMMA is hydrophobic, resistant to hydrolysis and is excreted without harmful effect to the human body. Due to its good mechanical properties, low cost, excellent biocompatibility and processability, PMMA has been widely adopted as bone cement. Moreover, PMMA deposition on orthopedic implants improves mechanical fixation and biological performance[16].

This work aimed to develop PLLA-PMMA-ALN filaments by extrusion and test the production of scaffolds via FDM-3DP. Seeking to understand the behavior of the blends and the influence of melting processing on the thermal stability of the mixtures, the filaments and scaffolds were characterized. The effort was to produce a dosage form for local administration of ALN, using relatively simple and innovative techniques such as extrusion and 3DP. As far as research has been carried out, there is no study using PLLA-PMMA-ALN blend in extrusion processing and 3DP.

2. Materials and Methods

PLLA was obtained from Nature Works 3D850 (0.5% of isomer D; density of 1.24 g/cm³; 176 °C melting point; 9 g (10 min⁻¹) to 210 °C with a load of 216 kg; average diameter of 2.8-2.9 mm), ALN trihydrate form was obtained from Alpex Healthcare Limited (Mw = 326,13 g/mol; 245 °C melting point) and PMMA was obtained from Sigma Aldrich (Mw = 15,000 g/mol; density 1.2 g/cm³).

In order to use all materials as a powder, PLLA was previously immersed in liquid nitrogen by 20 min and then inserted in a knife grinder per 5 min to obtain a thin powder[17]. In regard to limit PLLA degradation by hydrolysis in the mixtures, ALN trihydrate form was dry at 150 °C by 1 h in a vacuum oven at 350 mmHg to remove its hydration waters and, consequently, conversion into its anhydrous form[18].

2.1 Extrusion

Previously with each filament production, the samples were dried at 60 °C in a vacuum oven at 350 mmHg by 1 h for moisture removal and then inserted in a simply threaded mini extruder (Filmaq 3D CV). To produce the filaments. screw speed and nozzle temperature were maintained at 30 rpm and 185°C, respectively, for all the samples.

2.2 3D printing

The object model to be printed was obtained through 3D modeling software (Fusion 360, USA) and stored in STL file format. Slicing software (Ultimaker Cura, Netherlands) was used to plan the printing procedure; the file was saved to "G code" and imported into the 3D printer. A porous disc scaffolds were made on a 3D Printer (Creality CR-10S Pro brand) using the following print parameters: diameter: 25 mm, Mesh size: 1.5 mm and thickness:0.8 mm, at 180 °C

print temperature, 80 mm/s printing speed, 55 °C table temperature and 100% flow.

2.3 Techniques used for characterization

Filament and scaffolds samples were previously ground in a knife grinder, were analyzed by attenuated total reflectance infrared region with Fourier transform (ATR-FT-IR) (Frontier, Perkin Elmer) in the range of 4000-400 cm⁻¹, with a resolution of 4 cm⁻¹ and were an average of 32 repeated scans at room temperature.

Differential exploratory calorimetry (DSC) (DSC Q20, TA Instruments) curves were obtained under N_2 flow, employing sealed aluminum capsules containing about 5 mg of sample that were kept under heating from 25 to 200 °C, 1 min isotherm, a slow cooling up to -70 °C and a new heating up to 200 °C at a rate of 10 ° C min⁻¹. Given that PMMA possesses an amorphous structure and PLLA represents the principal component of mixtures, Equation 1[19] was employed to calculate the degree of polymer crystallinity (X_c) in the samples:

$$Xc(\%) = (1 / \varphi) \cdot \left(\Delta Hm / \Delta Hm^° \right) \cdot 100 \qquad (1)$$

where ΔH_m is the melting enthalpy, $\Delta H_m^°$ is the fusion enthalpy standard of a crystallinity sample of 100% and φ is the mass fraction of the polymer in the samples. PLLA standard melting enthalpy (ΔH_m) is 93.7 J/g[20]. Samples presenting more than one melting enthalpy, the total value in the equation ($\Delta H_{m1} + \Delta H_{m2} + \Delta H_{m3} + \Delta H_{m4}$) is inserted.

Previously cut into small pieces, were analyzed by X-ray diffractometry (DRX) (D8 Advance Eco, Bruker) in the two theta 2θ range from 2 to 50° range using an increase step 0.1 and permanence time of 1 sec at each step, in steps of 0.01°, at an accelerating voltage of 40 kV and a current of 25 mA under speed of 2° min⁻¹.

The filaments and scaffolds were cut into small pieces and prepared on carbon tape with gold deposition on their surface, creating a conductive film of electrons. The recovered samples were analyzed in the Scanning Electron Microscope with Field Emission (SEM-FEG) (Jeol, SM-71510 model) with a 10 kV electron-emitting beam. Measure of the pore size of the scaffolds occurred through the ImageJ software. Each mean diameter and standard deviation of filaments were obtained from the arithmetic average (5 measurements) in diameter at distant locations along the filaments with a digital caliper. To determine the average diameter of scaffold pores, Scaffold 1 took two measurements in each of the six pores visible in SEM-FEG image in 3 different micrographs; Scaffold 2 took two measurements in each of the two pores of 3 different photos.

3. Results and Discussions

A previous study found evidence of compatibility among binary and ternary physical mixtures of PLLA, PMMA, and drug polymers[21]. It showed the viability of producing filaments.

Table 1 shows that pure PLLA filament and Filaments 1, 5, and 9 have the lowest standard deviation values, indicating

a more constant diameter when compared to the filaments containing ALN, resulting from the favorable processability and miscibility of the PLLA-PMMA mixture.

The filaments containing ALN exhibited greater diameter measurement amplitudes and a mean value deviation of up to 0.29 mm from the standard extruder nozzle diameter (1.75 mm). It suggests that the extruder model utilized, with only one heating and feeding zone, may not be the most appropriate for these blends. The drug, with a T_m of 262 °C, higher than the processing temperature of 185 °C, is not melted with the other components, resulting in solid domains that increase shear stresses[22], making flow challenging during extrusion.

Significant variations in filament diameter can influence the subsequent 3D printing process of scaffolds, causing inconsistencies in the printed scaffold[23]. Concerning images of the manufactured filaments, Figure 1, the PLLA pure filament has an opaque white surface while PLLA-PMMA filaments have a lighter and more transparent appearance, suggesting miscibility, which is consistent with the diameter analysis of filaments. The presence of ALN turns the filaments whiter and opaque (trend of red arrows) as the amount of the drug increases. Filaments containing 20% and 25% of PMMA showed greater flexibility than other wires.

To monitor the impact of processing on filament degradation, Figure 2 in analysis demonstrated that the

870 cm^{-1} band, representing the crystalline area of PLLA[24], declined with a percentual increase of PMMA into the filaments (Figure 2A). Therefore, this polymer plays a role in decreasing the crystallinity of PLLA.

Most bands in the polymeric matrix remained in similar regions with no changes in chemical structure. However, the intensity of PLLA bands at 1750, 1128, and 1047 cm^{-1} (C=O) [18] and 1084 cm^{-1} (C-O-C)[25] (Figures 2B, 2C, and 2D) tend to increase with the incorporation of ALN. It is due to the presence of water molecules in the drug, which induces hydrolysis polymer degradation, and the contribution of thermal degradation during processing, which induces PLLA depolymerization[22]. Shortening polylactide molecules results in the formation of new carboxylic acid groups and affect the relative contributions of carbonyl (C=O), carbon-carbonyl-oxygen (C-CO-O), and oxygen-carbon-carbonyl (O-C-CO) groups. It was an effect observed in a preliminary compatibility study of the PLLA-ALN mixture[21].

The PMMA's typical bands at 1239 cm^{-1} (C-O), 1063, 987 and 841 cm^{-1} (C-C) and 1147 cm^{-1} (C-O-C)[24] were not observed in filaments (Figure 2B, 2C and 2D), partly due to the low intensity of these bands and the percentage of polymer in the filament (15-25%), and overlapping the intense PLLA band at 1084 cm^{-1} (C-O-C)[25]. Related to the stretching of the symmetric angular deformation group of

Table 1. The filaments nomenclature, composition, and mean diameter.

Name	Composition (wt%)	Weight (g)			Average Diameter (mm)
		PLLA	PMMA	ALN	
PLLA	PLLA (blank)	35.00	-	-	2.0 ± 0.08
Filament 1	PLLA+15%PMMA	35.00	5.25	-	1.46 ± 0.17
Filament 2	PLLA+15%PMMA+2.5%ALN	35.00	5.25	0.87	1.63 ± 0.18
Filament 3	PLLA+15%PMMA+5%ALN	35.00	5.25	1.75	1.68 ± 0.25
Filament 4	PLLA+15%PMMA+7.5%ALN	35.00	5.25	2.62	1.59 ± 0.21
Filament 5	PLLA+20%PMMA	35.00	7.00	-	1.75 ± 0.17
Filament 6	PLLA+20%PMMA+2.5%ALN	35.00	7.00	0.87	1.71 ± 0.10
Filament 7	PLLA+20%PMMA+5%ALN	35.00	7.00	1.75	1.55 ± 0.20
Filament 8	PLLA+20%PMMA+7.5%ALN	35.00	7.00	2.62	1.78 ± 0.20
Filament 9	PLLA+25%PMMA	35.00	8.75	-	1.90 ± 0.07
Filament 10	PLLA+25%PMMA+2.5%ALN	35.00	8.75	0.87	1.76 ± 0.12
Filament 11	PLLA+25%PMMA+5%ALN	35.00	8.75	1.75	1.84 ± 0.15
Filament 12	PLLA+25%PMMA+7.5%ALN	35.00	8.75	2.62	1.60 ± 0.15
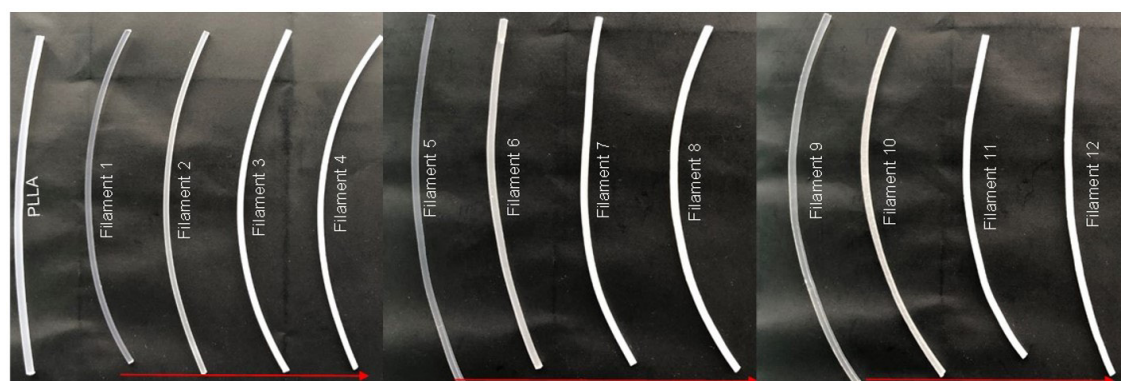
Figure 1. Images of the PLLA-PMMA filaments produced without and with ALN.
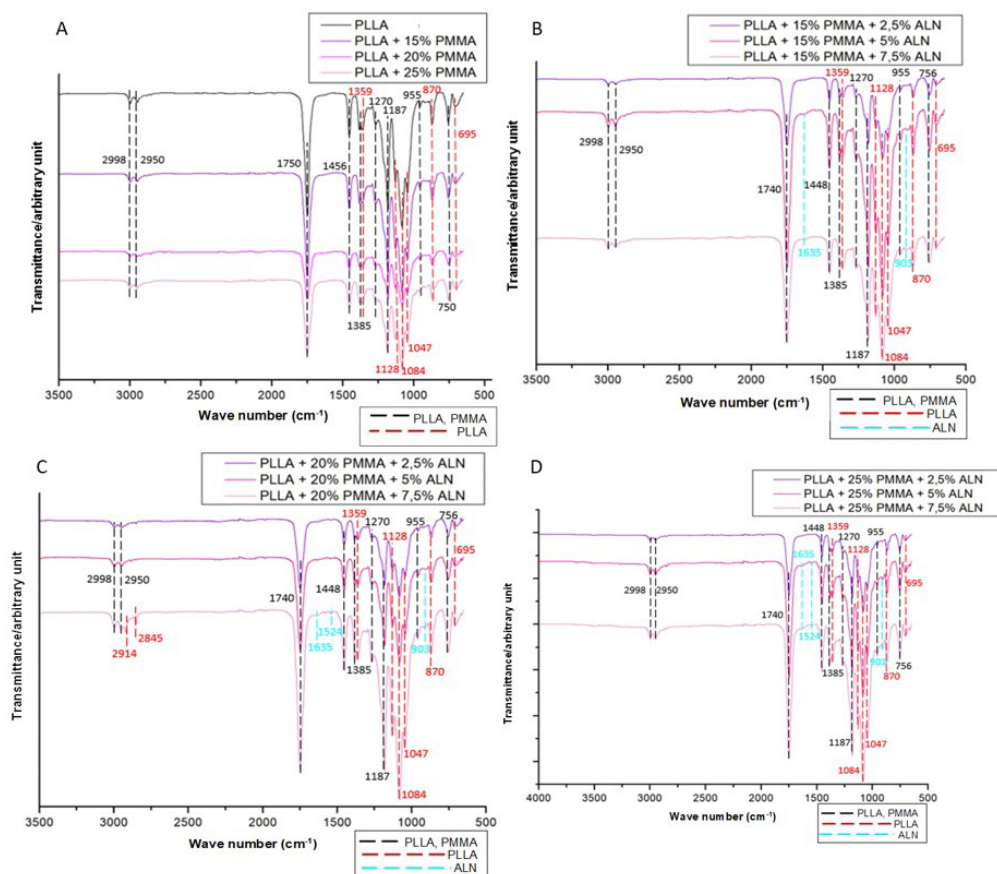
Figure 2. FTIR spectra obtained for the filaments produced. FTIR spectra of filaments: (A) PLLA containing 15, 20 and 25% of PMMA; (B) PLLA containing 15% of PMMA and different amounts of ALN; (C) PLLA containing 20% of PMMA and different amounts of ALN; (D) PLLA containing 25% of PMMA and different amounts of ALN.

PLLA are the bands at 2914 and 2845 cm^{-1} (Figure 2C)[25,26]. Based on this, the extruded did not show any blunt effects on the main functional groups of polymers, especially on PLLA.

In the filaments containing 5 and 7.5% ALN presented low absorption bands at 1635, 1524, and 903 cm^{-1} [27] (Figure 2B, 2C, and 2D), indicating the presence of drug crystals on their surface. These PLLA bands at 870 cm^{-1} are different from bands identified in the presence of PMMA. In this case, it increases with the incorporation of ALN, indicating its role as a nucleating agent[27]. Regarding the impact of extrusion on the filaments, Table 2 presents the data obtained from the DSC curves.

Pure PLLA filament exhibited T_m and T_g values (176.7 °C and 59.2 °C) that were like those observed for the untreated polymer (175.5 °C and 58.4 °C), suggesting that extrusion processing had insignificant effects on the thermal properties of PLLA. The filament with 25% PMMA exhibited the lowest melting point, resulting in a higher flow rate and facilitating melting processing[28].

The degree of crystallinity of the pure PLLA filament (19.4%) was slightly above the one found for gross material (13.4%), suggesting a favorable condition for crystal grow[29].

A progressive PMMA incorporation reduces the ΔH_m, and for filaments containing 20 and 25% of PMMA the second exothermic peak disappeared, which can be explained by PMMA's effect of restricting PLLA crystallization[30]. This result corroborates the reduction in T_g and the greater flexibility that these filaments showed. PLLA and Diphenyl-isocyanate (MDI) composites, processed by injection, showed similar T_g results[25].

The filament containing 15% PMMA and 5% ALN showed a decrease in crystallinity (20.9%) to the filament with 15% PMMA and 7.5% ALN (14.5%), despite the higher drug content. The domains of solid ALN's particles in the matrix may explain this reduction due to the formation of PLLA shapeless crystallites[31]. Filaments containing 25% PMMA and ALN also showed a slight decrease in crystallinity and melting enthalpy compared to filaments without ALN. A similar phenomenon was observed with the interfacial interaction of E-44 with the polymeric matrix (PET/PA-6), favoring nucleation but decreasing crystal growth[32].

Filaments containing 20% PMMA and either 5% or 7.5% ALN presented an increase in both crystallinity and ΔH_m relative to the filament that contained only PMMA. This outcome is expected with higher drug content; as higher crystallinity requires more energy during crystal fusion[18]. Filaments containing 15%, 20%, and 25% PMMA, with an increasing incorporation of ALN, exhibited

comparable T_m and T_g values. The lack of significant changes in T_m and T_g suggests no molecular interactions between the components during the extrusion process[13], and the drug had no direct effect on the thermal stability of the polymeric matrix.

The diffractograms obtained for the filaments (Figure 3) show for pure PLLA filament prominent peaks at 16° and 19°, with less intense peaks at 15° and 22°, similar to another study for PLLA/nHA filaments[33]. This result suggests increased crystallinity relative to the pure PLLA

Table 2. Summary of T_g, T_m, T_c, ΔH_m, ΔH_c and X_c values obtained from the DSC curves of the filaments produced.

Filament	T_g (°C)	T_{m1} (°C)	ΔH_{m1} (J/g)	T_{c1} (°C)	T_{c2} (°C)	ΔH_{c1} (J/g)	ΔH_{c2} (J/g)	X_c (%)
PLLA	59.2	176.7	48.9	92.9	160.3	24.8	5.9	19.4
PLLA+15%PMMA	58.3	176.4	46.5	95.5	161.4	28.2	4.1	17.6
PLLA+20%PMMA	56.9	175.7	39.1	104.4	-	30.1	-	11.6
PLLA+25%PMMA	56.7	174.6	38.3	106.9	-	29.3	-	12
PLLA+15%PMMA	58.3	176.4	46.5	95.5	161.4	28.2	4.1	17.6
PLLA+15%PMMA +2.5%ALN	58.6	176.4	45.2	98.2	162.9	28.2	3.8	16.6
PLLA+15%PMMA +5%ALN	55.1	174.7	37.5	100.2	-	21.2	-	20.9
PLLA+15%PMMA +7.5%ALN	56.7	176.2	40.5	96.2	162.4	27.3	2.2	14.5
PLLA+20%PMMA	56.9	175.7	39.1	104.4	-	30.1	-	11.6
PLLA+20%PMMA +2.5%ALN	56.3	174.9	38.6	101.5	-	30.5	-	10.7
PLLA+20%PMMA +5%ALN	56.9	176	41.6	99.1	163.1	31.4	1.1	12.1
PLLA+20%PMMA +7.5%ALN	56.2	174.5	40.5	111.9	-	28.9	-	15.9
PLLA+25%PMMA	56.7	174.6	38.3	106.9	-	29.3	-	12
PLLA+25%PMMA +2.5%ALN	57.1	175.8	29.8	103.5	-	24.1	-	7.8
PLLA+25%PMMA 5%ALN	57.1	175.1	37.1	101.5	-	29.1	-	11.2
PLLA+25%PMMA +7.5%	57.9	176.8	22.5	102.8	-	17.5	-	7.1
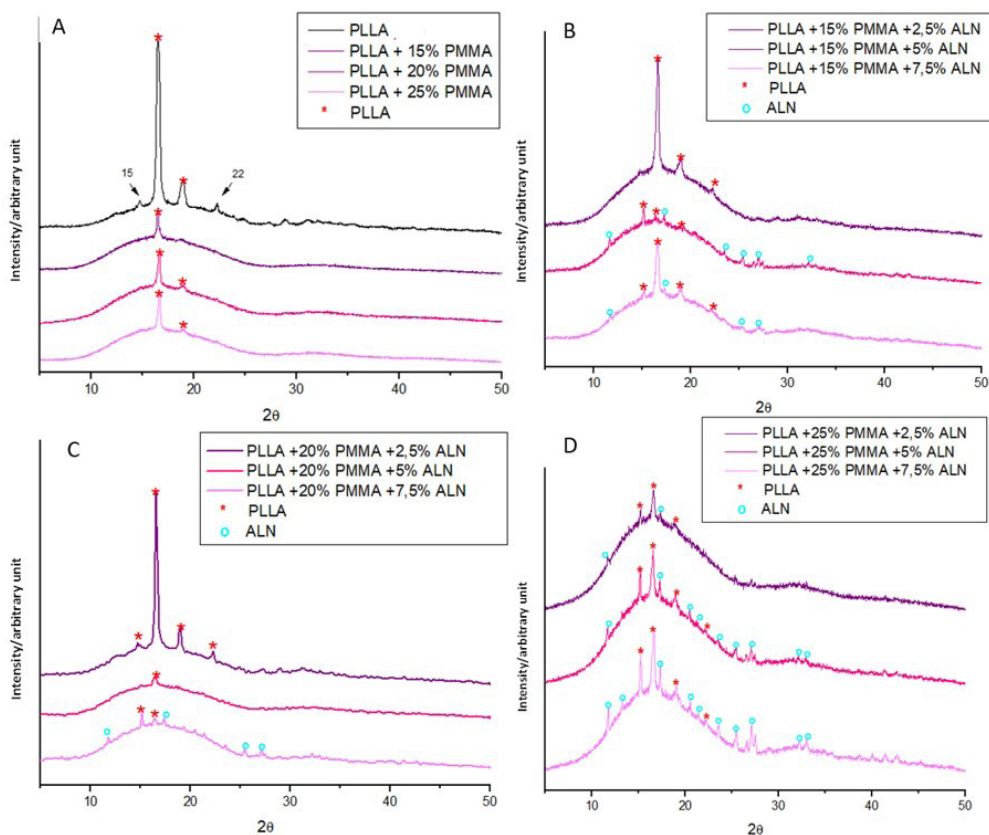
Figure 3. Diffractogram obtained for the produced filaments. *Diffractogram of filaments: (A) PLLA containing 15, 20 and 25% of PMMA; (B) PLLA containing 15% of PMMA and different amounts of ALN; (C) PLLA containing 20% of PMMA and different amounts of ALN; (D) PLLA containing 25% of PMMA and different amounts of ALN.

presented in the DSC analysis. The presence of PMMA in filaments increases the amorphous halo, keeping in line with the FTIR and DSC results. All filaments exhibited a semi-crystalline nature (figures-3B, 3C, and 3D) with the presence of ALN peaks in the filaments containing 5 and 7.5% of the drug and 15% PMMA. The lack of these peaks in the filament with only 2.5% of ALN can be explained by the low concentration of the drug, with its crystalline region below the detection limits of the assay[9].

Filaments with 20% PMMA exhibit ALN peaks exclusively in the filament containing 7.5% ALN. The filament with 5% ALN did not show these peaks, even though the FTIR spectrum and SEM-FEG images suggested the presence of the drug. These results indicate that there were no drug crystals on the surface in the analyzed sample, as XRD analysis lacks the ability to detect crystals in the sample's penetration depth[34]. Filaments containing 25% PMMA show a notable rise in PLLA characteristic peaks as drug concentration increases. ALN, a nucleation agent, hindering molecular chain movement and inducing polymeric matrix crystallinity[35]. These results contradict the crystallinity found in the DSC analysis.

Through visual analysis and in SEM-FEG, Figure 4 (red arrows), white crystals ALN were observable in the 5 to 7.5% ALN filaments, confirming its homogeneous dispersion on those surfaces and by results where ALN bands appear on the filaments. As the concentration of ALN increases, the roughness and deformations (highlighted in red) also increase. This finding aligns with the results obtained from visual and diameter analyses of the filaments.

Pure PLLA filament exhibits a smooth surface without substantial deformation (figure -4A), observed during the PLA/F68 implant production[4]. Furthermore, the surface of PLLA-PMMA filaments becomes smoother and without roughness as the percentage of PMMA increases, showing good interfacial compatibility[30]. The ability of PMMA to facilitate flow during extrusion and the miscibility of the PLLA/PMMA blend are the answers.

Considering that filaments containing 25% PMMA showed: i) more constant diameter facilitating 3DP processing; ii) greater material flexibility and processability and iii) lower crystallinity degree when compared to other ALN filaments, which positively impacts the mechanical properties and the degradation rate of the polymeric matrix, filament 10 (25% PMMA+2.5% ALN) and filament 12 (25% PMMA+7.5% ALN) were selected for scaffolds 3DP, Figure 5.
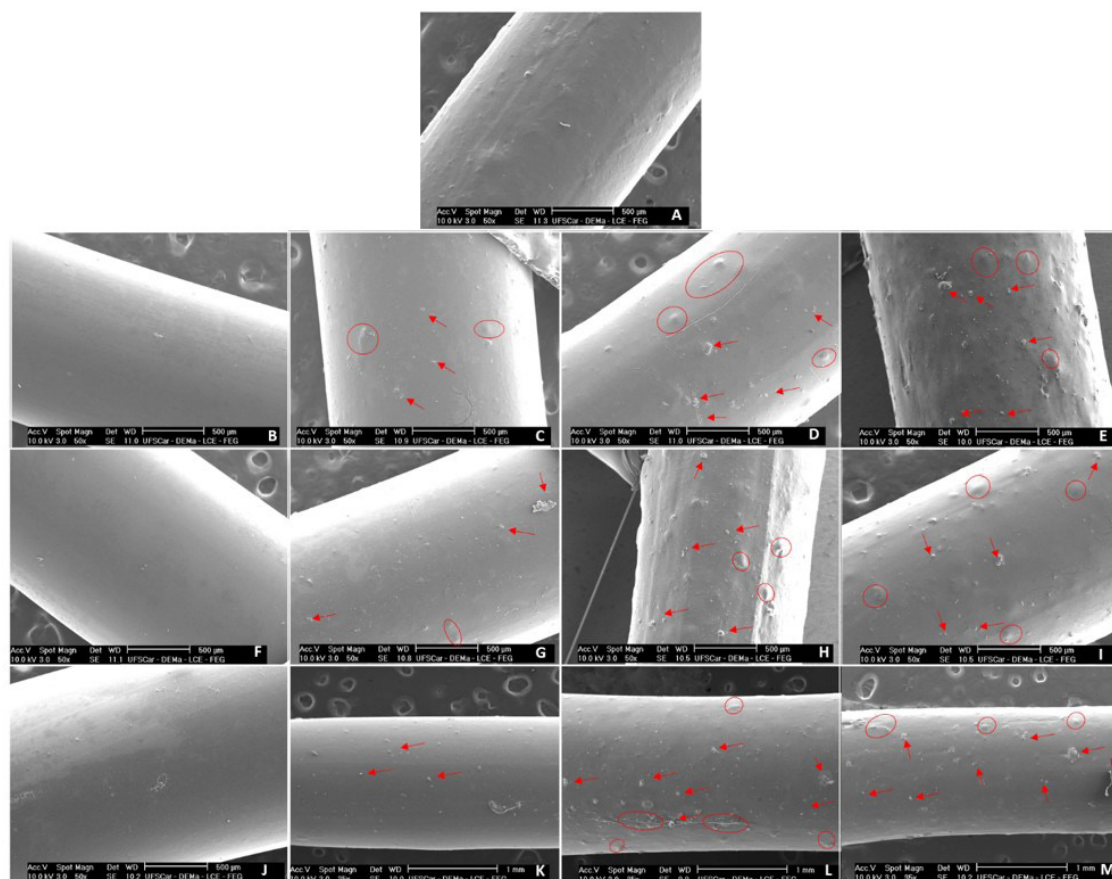
Figure 4. Micrographs of the PLLA-PMMA filaments obtained by SEM-FEG. SEM images of filaments: (A) PLLA; (B) PLLA+15%PMMA; (C) PLLA+15%PMMA+2.5%ALN; (D) PLLA+15%PMMA+5%ALN; (E) PLLA+15%PMMA+7.5%ALN; (F) PLLA+20%PMMA; (G) PLLA+20%PMMA+2.5%ALN; (H) PLLA+20%PMMA+5%ALN; (I) PLLA+20%PMMA+7.5%ALN; (J) PLLA+25%PMMA; (K) PLLA+25%PMMA+2.5%ALN; (L) PLLA+25%PMMA+5%ALN; (M) PLLA+25%PMMA+7.5%ALN.

Scaffolds presented geometry according to the design. Scaffold 1 has a stable structure without deformations, while scaffold 2 shows remnants of the polymer adhered to its surface. The filament diameter variation was responsible for printing inconsistencies[23].

From the SEM images in Figure 6, it is possible to observe that the scaffolds have a porous structure (arrows in Figure 6A and 6C) regular and connected, and drug crystals (arrows in Figure 6B and 6D) dispersed relatively homogeneously in both scaffolds. A homogeneous dispersion
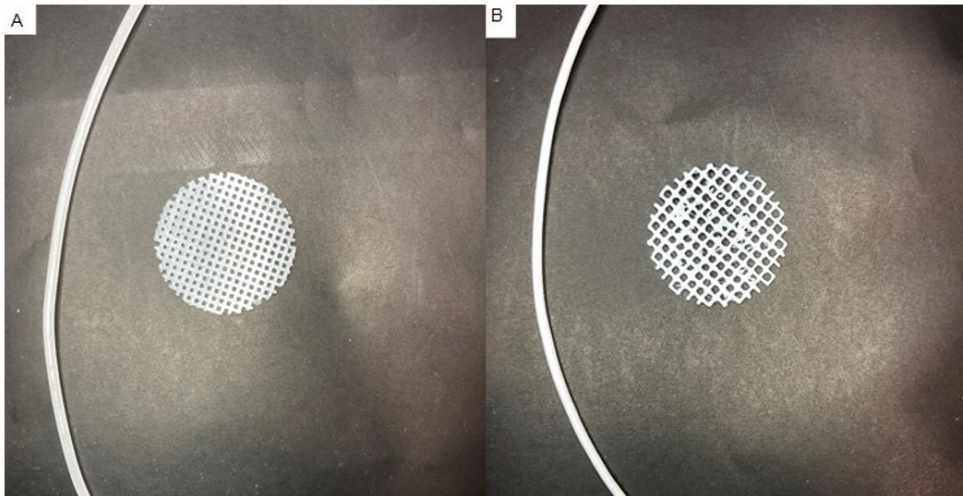
Figure 5. Scaffolds images produced from filament 10 containing 25% PMMA and 2.5% ALN (A) and filament 12 containing 25% PMMA and 7.5% ALN (B).
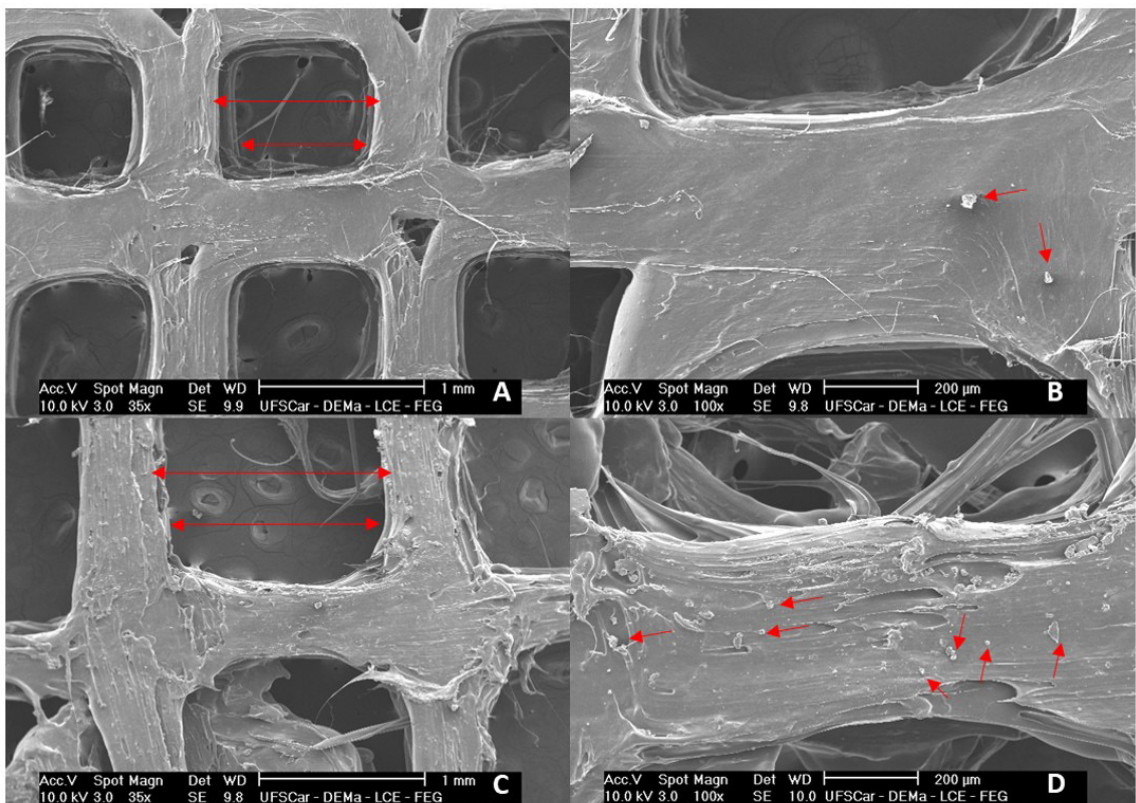
Figure 6. The SEM-FEG micrographs from scaffolds 1 and 2. SEM images of scaffolds: scaffold 1 (PLLA+25%PMMA+2.5%ALN) with bar = 1mm (A) and bar = 200 μm (B); scaffold 2 (PLLA+25%PMMA+7.5%ALN) with bar = 1 mm (C) and bar = 200 μm (D).
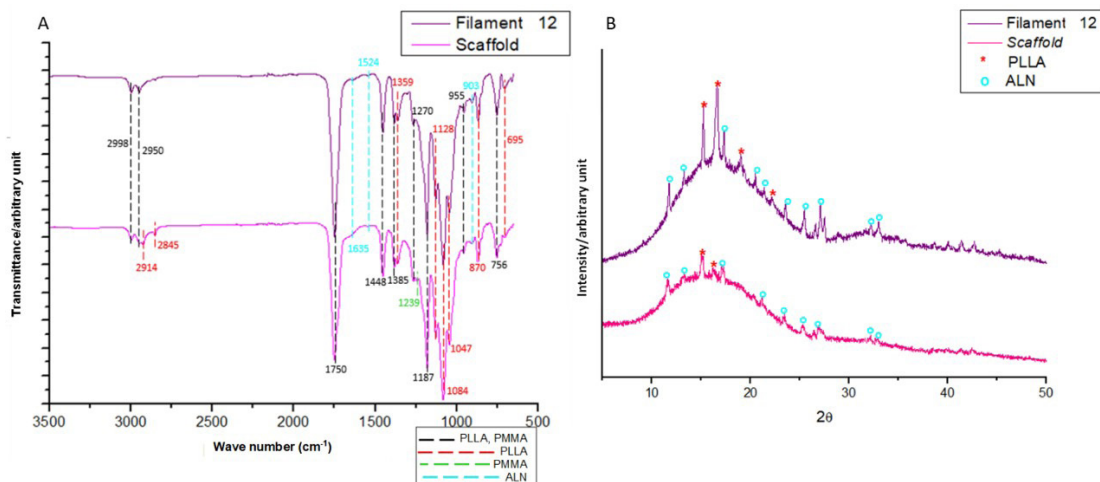
Figure 7. FTIR (A) and diffractogram spectra (B) obtained for Filament 12 and Scaffold 2.

Table 3. Data obtained from DSC curves for filaments 12 and scaffold produced from it.

Sample	T_g (°C)	T_{m1} (°C)	ΔH_{m1} (J/g)	T_{c1} (°C)	T_{c2} (°C)	ΔH_{c1} (J/g)	ΔH_{c2} (J/g)	X_c (%)
Filament PLLA+25%PMMA+7.5%ALN	57.9	176.8	22.5	102.8	-	17.5	-	7.1
Scaffold PLLA+25%PMMA+7.5%ALN	57.2	175.3	35.7	101.8	-	27.5	-	11.6

of crystals is important because the presence of crystal clusters can concentrate tension points on the structure which leads to fragility of material[17]. Scaffold 2 showed increased surface roughness and deformations due to its higher drug concentration.

Considering the diameter of the pores, scaffold 1 showed an average diameter of 0.84 mm (840 µm), a value relatively close to the one determined (1 mm). For scaffold 2, the mean diameter obtained was 1.37 mm (1370 µm), short of the desired 1.5 mm. Both scaffolds presented micropores larger than 200 µm, that are considered ideal for bone regeneration[36]. Since a porous scaffold structure provides a biological environment that promotes cell adhesion, tissue proliferation and growth, and allows nutrient flow[37].

The scaffold results suggest that the amount of API used influences the 3DP process, which agrees with literature[38]. Applying porous diameter as a parameter, scaffold 2 is a more exciting alternative, being selected for investigation in the following analysis. Besides, the higher ALN content helps to analyze the effect of the FDM-3DP on the chemical, physical, and thermal material stability. Figure 7 presents the FTIR spectra and diffractograms obtained for filament 12 and scaffold 2.

The spectrum indicates that filament and scaffold exhibited similar behavior (Figure 7A). Notably, the PMMA band at 1239 cm⁻¹ (C-O), absent in the filament, was visible in the scaffold at a low intensity. The appearance of this band might be related to the alteration in the intensity of PLLA bands at 1750 cm⁻¹ (C=O), 1084 cm⁻¹ (C-O-C), 1128, and 1047 cm⁻¹ (C-O) in the scaffold. These bands are susceptible to change due to polymer degradation[26], probably caused by subsequent thermal degradation after extrusion and 3DP.

The scaffold presents bands at 2914 and 2845 cm⁻¹ attributed to the stretching of PLLA symmetrical angular deformation group[25,26]. Furthermore, PLLA and ALN peaks are visible in both the scaffold and the filament (Figure 7B), wherein the reduction of these peaks indicates a relative decrease of crystallinity in the scaffold, contradicting the DSC analysis.

From the DSC results, Table 3, filament and scaffold showed similar T_m and T_g values, suggesting no molecular interactions during 3D printing processing[13]. An increase from 7.1 to 11.6% in crystallinity was observed, indicating favored crystallinity in 3DP[29], as observed in extrusion. Composites of PLA and tricalcium phosphate processed by extrusion[39] with a similar behavior presented adequate mechanical properties for scaffolds. There was also an increase in ΔH_m of 22.5 J/g in filament to 35.7 J/g in scaffold, an expected result because the bigger the crystallinity, more energy is consumed in the fusion of crystals, making it challenging to change the phase of polymeric matrix[17].

4. Conclusions

During extrusion, the properties of the components were maintained. The presence of ALN as solid crystals, attributed roughness, and deformations in filaments. It was also found that PMMA reduced crystallinity in the PLLA matrix and improved flow during processing and malleability to filaments. This result may positively influence the polymeric matrix's mechanical properties and degradation rate in human body and assist in later 3DP processing. Based on set of results, the filaments containing 25%PMMA and 2.5% and 7.5% of ALN were selected to produce scaffolds.

In the second part of the study, it was possible to produce PLLA/PMMA/ALN filaments by extrusion and scaffolds by accurate 3DP, mainly the PLLA+25%PMMA+7.5%ALN with good physicochemical properties for bone tissue engineering aiming at local drug release. Drug release studies from the mixtures presented here will be conducted in further papers.

5. Author's Contribution

Conceptualization – Olivia Deretti; Denise Abatti Kasper Silva; Ana Paula Testa Pezzin.

Data curation – Olivia Deretti; Denise Abatti Kasper Silva; Ana Paula Testa Pezzin.

Formal analysis – Olivia Deretti; Lucas Werner; Luana Engelmann; Denise Abatti Kasper Silva; Ana Paula Testa Pezzin.

Funding acquisition – Denise Abatti Kasper Silva; Ana Paula Testa Pezzin.

Investigation – Olivia Deretti; Guilherme Tait; Lucas Werner.

Methodology – Olivia Deretti; Denise Abatti Kasper Silva; Ana Paula Testa Pezzin.

Project administration – Denise Abatti Kasper Silva; Ana Paula Testa Pezzin.

Resources – Lucas Werner; Denise Abatti Kasper Silva; Ana Paula Testa Pezzin.

Software – Lucas Werner.

Supervision – Olivia Deretti; Denise Abatti Kasper Silva; Ana Paula Testa Pezzin.

Validation – Olivia Deretti; Denise Abatti Kasper Silva; Ana Paula Testa Pezzin.

Visualization – Olivia Deretti; Denise Abatti Kasper Silva; Ana Paula Testa Pezzin.

Writing – original draft – Olivia Deretti.

Writing – review & editing – Olivia Deretti; Denise Abatti Kasper Silva; Ana Paula Testa Pezzin.

6. Acknowledgements

7. References

1. Tarafder, S., & Bose, S. (2014). Polycaprolactone-coated 3D printed tricalcium phosphate scaffolds for bone tissue engineering: in vitro alendronate release behavior and local delivery effect on in vivo osteogenesis. *ACS Applied Materials & Interfaces*, *6*(13), 9955-9965. http://doi.org/10.1021/am501048n. PMid:24826838.

2. Posadowska, U., Parizek, M., Filova, E., Wlodarczyk-Biegun, M., Kamperman, M., Bacakova, L., & Pamula, E. (2015). Injectable nanoparticle-loaded hydrogel system for local delivery of sodium alendronate. *International Journal of Pharmaceutics*, *485*(1-2), 31-40. http://doi.org/10.1016/j.ijpharm.2015.03.003. PMid:25747455.

3. Mir, M., Ahmed, N., & Rehman, A. (2017). Recent applications of PLGA based nanostructures in drug delivery. *Colloids and Surfaces. B, Biointerfaces*, *159*, 217-231. http://doi.org/10.1016/j.colsurfb.2017.07.038. PMid:28797972.

4. Li, D., Guo, G., Deng, X., Fan, R., Guo, Q., Fan, M., Liang, J., Luo, F., & Qian, Z. (2013). PLA/PEG-PPG-PEG/Dexamethasone implant prepared by hot-melt extrusion for controlled release of immunosuppressive drug to implantable medical devices, part 2: in vivo evaluation. *Drug Delivery*, *20*(3-4), 134-142. http://doi.org/10.3109/10717544.2013.801049. PMid:23745720.

5. Wang, Y., Sun, L., Mei, Z., Zhang, F., He, M., Fletcher, C., Wang, F., Yang, J., Bi, D., Jiang, Y., & Liu, P. (2020). 3D printed biodegradable implants as an individualized drug delivery system for local chemotherapy of osteosarcoma. *Materials & Design*, *186*, 108336. http://doi.org/10.1016/j.matdes.2019.108336.

6. Awad, A., Fina, F., Goyanes, A., Gaisford, S., & Basit, A. W. (2021). Advances in powder bed fusion 3D printing in drug delivery and healthcare. *Advanced Drug Delivery Reviews*, *174*, 406-424. http://doi.org/10.1016/j.addr.2021.04.025. PMid:33951489.

7. Jamróz, W., Kurek, M., Łyszczarz, E., Brniak, W., & Jachowicz, R. (2017). Printing techniques: recent developments in pharmaceutical technology. *Acta Poloniae Pharmaceutica - Drug Research*, *74*(3), 753-763. PMid:29513944.

8. Goole, J., & Amighi, K. (2016). 3D printing in pharmaceutics: a new tool for designing customized drug delivery systems. *International Journal of Pharmaceutics*, *499*(1-2), 376-394. http://doi.org/10.1016/j.ijpharm.2015.12.071. PMid:26757150.

9. Goyanes, A., Allahham, N., Trenfield, S. J., Stoyanov, E., Gaisford, S., & Basit, A. W. (2019). Direct powder extrusion 3D printing: fabrication of drug products using a novel single-step process. *International Journal of Pharmaceutics*, *567*, 118471. http://doi.org/10.1016/j.ijpharm.2019.118471. PMid:31252147.

10. Danda, L. J. A., Batista, L. M., Melo, V. C. S., Soares Sobrinho, J. L., & Soares, M. F. L. R. (2019). Combining amorphous solid dispersions for improved kinetic solubility of posaconazole simultaneously released from soluble PVP/VA64 and an insoluble ammonio methacrylate copolymer. *European Journal of Pharmaceutical Sciences*, *133*, 79-85. http://doi.org/10.1016/j.ejps.2019.03.012. PMid:30890364.

11. Sayanjali, S., Sanguansri, L., Ying, D., Buckow, R., Gras, S., & Augustin, M. A. (2019). Extrusion of a curcuminoid-enriched oat fiber-corn-based snack product. *Journal of Food Science*, *84*(2), 284-291. http://doi.org/10.1111/1750-3841.14432. PMid:30648743.

12. Domínguez-Robles, J., Martin, N. K., Fong, M. L., Stewart, S. A., Irwin, N. J., Rial-Hermida, M. I., Donnelly, R. F., & Larrañeta, E. (2019). Antioxidant PLA composites containing lignin for 3d printing applications: a potential material for healthcare applications. *Pharmaceutics*, *11*(4), 165. http://doi.org/10.3390/pharmaceutics11040165. PMid:30987304.

13. Boetker, J., Water, J. J., Aho, J., Arnfast, L., Bohr, A., & Rantanen, J. (2016). Modifying release characteristics from 3D printed drug-eluting products. *European Journal of Pharmaceutical Sciences*, *90*, 47-52. http://doi.org/10.1016/j.ejps.2016.03.013. PMid:26987609.

14. Tyler, B., Gullotti, D., Mangraviti, A., Utsuki, T., & Brem, H. (2016). Polylactic acid (PLA) controlled delivery carriers for biomedical applications. *Advanced Drug Delivery Reviews*, *107*, 163-175. http://doi.org/10.1016/j.addr.2016.06.018. PMid:27426411.

15. Anakabe, J., Orue, A., Huici, A. M. Z., Eceiza, A., & Arbelaiz, A. (2018). Properties of PLA/PMMA blends with high polylactide content prepared by reactive mixing in presence

of poly (styrene-co-glycidyl methacrylate) copolymer. *Journal of Applied Polymer Science*, *135*(43), 46825. http://doi.org/10.1002/app.46825.

16. Camargo, E., Serafim, B. M., Cruz, A. F., Soares, P., Oliveira, C. C., Saul, C. K., & Marino, C. E. B. (2021). Bioactive response of PMMA coating obtained by electrospinning on ISO5832-9 and Ti6Al4V biomaterials. *Surface and Coatings Technology*, *412*, 127033. http://doi.org/10.1016/j.surfcoat.2021.127033.

17. Siqueira, A. (2018). *Obtenção de scaffolds poliméricos baseados em poli (ácido láctico), hidroxiapatita e óxido de grafeno utilizado o método de manufatura aditiva por "fused deposition modelling"* (Master's dissertation). Universidade Presbitariana Mackenzie, São Paulo.

18. Asnani, M., Vyas, K., Bhattacharya, A., Devarakonda, S., Chakraborty, S., & Mukherjee, A. K. (2009). Ab initio structure determination of anhydrous sodium alendronate from laboratory powder X-ray diffraction data. *Journal of Pharmaceutical Sciences*, *98*(6), 2113-2121. http://doi.org/10.1002/jps.21561. PMid:18781644.

19. Silva-Buzanello, R. A., Souza, M. F., Oliveira, D. A., Bona, E., Leimann, F. V., Cardozo, L., Fo., Araújo, P. H. H., Ferreira, S. R. S., & Gonçalves, O. H. (2016). Preparation of curcumin-loaded nanoparticles and determination of the antioxidant potential of curcumin after encapsulation. *Polímeros*, *26*(3), 207-214. http://doi.org/10.1590/0104-1428.2246.

20. Garlotta, D. (2001). A literature review of poly (lactic acid). *Journal of Polymers and the Environment*, *9*(2), 63-84. http://doi.org/10.1023/A:1020200822435.

21. Deretti, O. (2022). *Novos filamentos biorreabsorvíveis para scaffolds visando a administração local de alendronato de sódio* (Master's dissertation). Universidade da Região de Joinville, Joinville.

22. Cifuentes, S. C., Lieblich, M., Lopez, F. A., Benavente, F., & Gonzáles-Carrasco, J. L. (2017). Effect of Mg content on the thermal stability and mechanical behaviour of PLLA/Mg composites processed by hot extrusion. *Materials Science and Engineering C*, *72*, 18-25. http://doi.org/10.1016/j.msec.2016.11.037. PMid:28024575.

23. Water, J. J., Bohr, A., Boetker, J., Aho, J., Sandler, N., Nielsen, H. M., & Rantanen, J. (2015). Three-dimensional printing of drug-eluting implants: preparation of an antimicrobial polylactide feedstock material. *Journal of Pharmaceutical Sciences*, *104*(3), 1099-1107. http://doi.org/10.1002/jps.24305. PMid:25640314.

24. Yuniarto, K., Purwanto, Y. A., Purwanto, S., Welt, B. A., Purwadaria, H. K., & Sunarti, T. C. (2016). Infrared and Raman studies on polylactide acid and polyethylene glycol-400 blend. *AIP Conference Proceedings*, *1725*(1), 020101. http://doi.org/10.1063/1.4945555.

25. Bitencourt, S. S., Batista, K. C., Zattera, A. J., Silva, D. A. K., & Pezzin, A. P. T. (2017). Development of poly (L-lactic acid PLLA) biocomposites with waste wood. *Revista Matéria*, *22*(4), e11899.

26. Ferrández-Montero, A., Lieblich, M., Benavente, R., Gonzáles-Carrasco, J. L., & Ferrari, B. (2020). Study of the matrix-filler interface in PLA/Mg composites manufactured by material extrusion using a colloidal feedstock. *Additive Manufacturing*, *33*, 101142. http://doi.org/10.1016/j.addma.2020.101142.

27. Oz, U. C., Küçüktürkmen, B., Devrim, B., Saka, O. M., & Bozkir, A. (2019). Development and optimization of alendronate sodium loaded PLGA nanoparticles by central composite design. *Macromolecular Research*, *27*(9), 857-866. http://doi.org/10.1007/s13233-019-7119-z.

28. Wang, S., Capoen, L., D'Hooge, D. R., & Cardon, L. (2018). Can the melt flow index be used to predict the success of fused deposition modelling of commercial poly (lactic acid) filaments into 3D printed materials? *Plastics, Rubber and Composites*, *47*(1), 9-16. http://doi.org/10.1080/14658011.2017.1397308.

29. Silveira, E. (2015). *Estudo da tenacificação do PLA pela adição de elastômero termoplástico EMA-GMA* (Master's dissertation). Escola Politécnica, Universidade de São Paulo, São Paulo.

30. Ju, J., Peng, X., Huang, K., Li, L., Liu, X., Chitrakar, C., Chang, L., Gu, Z., & Kuang, T. (2019). High-performance porous PLLA-based scaffolds for bone tissue engineering: Preparation, characterization, and in vitro and in vivo evaluation. *Polymer*, *180*, 121707. http://doi.org/10.1016/j.polymer.2019.121707.

31. Agüero, Á., Garcia-Sanoguera, D., Lascano, D., Rojas-Lema, S., Ivorra-Martinez, J., Fenollar, O., & Torres-Giner, S. (2020). Evaluation of different compatibilization strategies to improve the performance of injection-molded green composite pieces made of polylactide reinforced with short flaxseed fibers. *Polymers*, *12*(4), 821. http://doi.org/10.3390/polym12040821. PMid:32260439.

32. Huang, Y., Liu, Y., & Zhao, C. (1998). Morphology and properties of PETE/PA-6/E-44 blends. *Journal of Applied Polymer Science*, *69*(8), 1505-1515. http://doi.org/10.1002/(SICI)1097-4628(19980822)69:8<1505::AID-APP4>3.0.CO;2-G.

33. Delabarde, C., Plummer, C. J. G., Bourban, P.-E., & Manson, J.-A. E. (2010). Solidification behaviour of PLLA/nHA nanocomposites. *Composites Science and Technology*, *70*(13), 1813-1819. http://doi.org/10.1016/j.compscitech.2010.04.024.

34. Haser, A., Huang, S., Listro, T., White, D., & Zhang, F. (2017). An approach for chemical stability during melt extrusion of a drug substance with a high melting point. *International Journal of Pharmaceutics*, *524*(1-2), 55-64. http://doi.org/10.1016/j.ijpharm.2017.03.070. PMid:28359810.

35. Srivastava, A., Ahuja, R., Bhati, P., Singh, S., Chauhan, P., Vashisth, P., Kumar, A., & Bhatnagar, N. (2020). Fabrication and characterization of PLLA/Mg composite tube as the potential bioresorbable/biodegradable stent (BRS). *Materialia*, *10*, 100661. http://doi.org/10.1016/j.mtla.2020.100661.

36. Wu, W., Zheng, Q., Guo, X., & Huang, W. (2009). The controlled-releasing drug implant based on the three-dimensional printing technology: fabrication and properties of drug implant. *Journal Wuhan University of Technology-Materials Science Edition*, *24*(6), 977-981. http://doi.org/10.1007/s11595-009-6977-1.

37. Rosiak, P., Latanska, I., Paul, P., Sujka, W., & Kolesinska, B. (2021). Modification of alginates to modulate their physico-chemical properties and obtain biomaterials with different functional properties. *Molecules*, *26*(23), 7264. http://doi.org/10.3390/molecules26237264. PMid:34885846.

38. Tidau, M., Kwade, A., & Finke, J. H. (2019). Influence of high, disperse API load on properties along the fused-layer modeling process chain of solid dosage forms. *Pharmaceutics*, *11*(4), 194. http://doi.org/10.3390/pharmaceutics11040194. PMid:31013578.

39. Drummer, D., Cifuentes-Cuélar, S., & Rietzel, D. (2012). Suitability of PLA/TCP for fused deposition modeling. *Rapid Prototyping Journal*, *18*(6), 500-507. http://doi.org/10.1108/13552541211272045.